Macromolecules

Article

pubs.acs.org/Macromolecules

Effect of Ca^{2+} Ion and Temperature on Association of Thermally Sensitive PAA-*b*-PNIPAM Diblock Chains in Aqueous Solutions

Xiaobing Liu,[†] Shikai Luo,[‡] Jing Ye,[†] and Chi Wu*[,†,§]

[†]Hefei National Laboratory for Physical Sciences at Microscale, Department of Chemical Physics, University of Science and Technology of China, Hefei, China 230026

[‡]Institute of Chemical Materials, China Academy of Engineering Physics, Mianyang, China 621900

[§]Department of Chemistry, The Chinese University of Hong Kong, Shatin N. T., Hong Kong

Supporting Information

ABSTRACT: Poly(*tert*-butyl acrylate)-*b*-poly(*N*-isopropylacrylamide) (PtBA-*b*-PNIPAM) was first synthesized by sequential reversible addition−fragmentation chain transfer polymerization of *tert*-butyl acrylate and *N*-isopropylacrylamide. Its hydrolysis led to amphiphilic poly(acrylic acid)-*b*-poly(*N*-isopropylacrylamide) (PAA-*b*-PNIPAM) that can form micelles in aqueous solutions at temperatures higher than 37 °C because PNIPAM is a thermally sensitive polymer. In the presence of Ca^{2+}, the complexation between one Ca^{2+} and two COO^- groups on different PAA blocks can induce the chain association. Using a combination of static and dynamic laser light scattering, we studied the effect of Ca^{2+} and temperature as well as the sequence of adding Ca^{2+} ions and heating the solution on such association. We found that (1) the association is controllable and reversible, (2) a distinct hysteresis is observed between the heating and cooling processes, (3) the time evolution of the average aggregation number (N_{agg}) and the average hydrodynamic radius ($\langle R_h \rangle$) of the aggregates can be expressed by a single-exponential equation, (4) the aggregates have a fractal dimension of 1.5−1.9, suggesting a diffusion-limited process, and (5) adding Ca^{2+} before heating results in the aggregates with a more open and looser structure. The current study provides a model system to investigate a more complicate problem, namely, the effect of metal ions on the stability of protein chains.

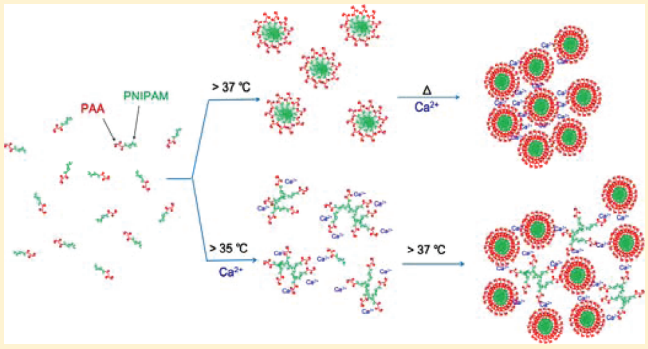

INTRODUCTION

The self-association of amphiphilic block copolymer chains in selective solvents to form stable aggregates with various structures have been extensively studied and used in numerous potential applications, including the solubilization of drugs, water purification, nanoreactors, and potential vectors for gene transfection.[1−5] The copolymers with one polyelectrolytes block combine structural features of polyelectrolytes and surfactants and have special properties, which have attracted much attention in recent years.[6] On the other hand, the complexation of cationic metal ions with charged polymer chains commonly occurs in different applications of polyelectrolytes, ranging from detergents to water treatment and in biological systems. Recent studies showed that Cu^{2+} binds to prion proteins and plays an important biological function.[7] Some even suggested that it might be linked to the progression of prion-mediated disease because epidemiological studies of clusters of prion disease showed these locations have a low soil concentration of copper.[8,9] Therefore, a better understanding of how charged macromolecules complex with metal ions at the molecular level becomes essential in the studies of their physicochemical behavior in environmental and biological systems.

Much theoretical[10−13] and experimental[14−17] effort has been devoted to the understanding of the formation and structure of colloidal aggregation. In general, there are two limited cases: namely, the diffusion-limited cluster−cluster aggregation (DLCA) and the reaction-limited cluster−cluster aggregation (RLCA),[18] in which the sticking efficiencies (probabilities) of two colliding objects are close to 100% (irreversible collision) or very low (many collisions result in one sticking, just like chemical reactions), respectively. Different aggregation processes lead to different fractal dimensions (d_f) of the resultant aggregates, i.e., $M \sim R^{d_f}$, where M and R are their mass and size, respectively. The DLCA process leads to the formation of the aggregates with an open and less uniform structure with $d_f \sim 1.75-1.80$ in three dimensions, while the aggregates formed in the RLCA process are structurally more uniform with a higher fractal dimension ($d_f \sim 2.0$). The kinetics of DLCA is characterized by a power law $R \sim t^{\alpha}$ with $\alpha < 1$, where t is the aggregation time.[19] A combination of different scattering

Received: March 29, 2012
Revised: May 13, 2012
Published: May 22, 2012

Scheme 1. Synthesis of Thermally Sensitive PAA-*b*-PNIPAM Diblock Copolymer

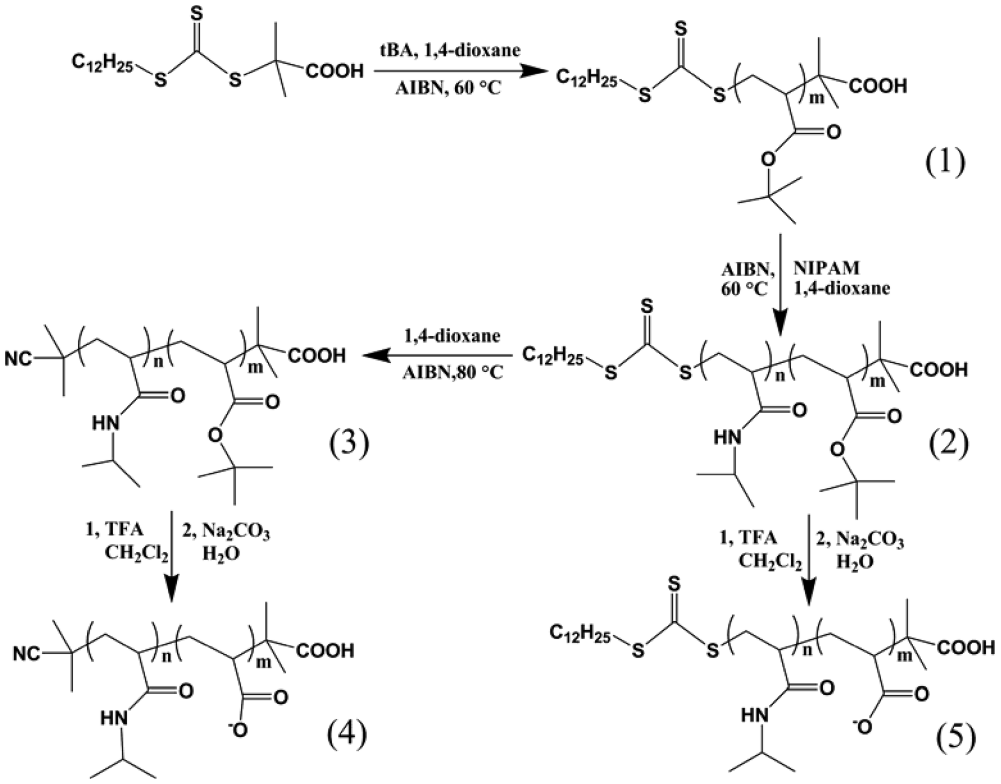

techniques was used to study the formation and structure of the aggregates over a wide size range.[20−24]

For colloidal systems, the sticking probability is often changed by adding some salts to destabilize colloidal particles, while for polymeric systems, the choice is more, such as the variation of pH and temperature. For example, poly(acrylic acid) as a weak polyelectrolytes can change its chain conformation when the ionic strength or pH is alternated because the protonation−deprotonation equilibrium of its carboxylate groups in aqueous solution.[25] Note that changing pH or adding salts faces an intrinsic problem of how to uniformly alternate pH or the salt concentration in a dispersion or solution. Such a problem is often neglected in the literature. In comparison, the solution or dispersion temperature can be uniformly adjusted. Among thermally sensitive polymers, poly(*N*-isopropylacrylamide) (PNIPAM) with an easily accessible lower critical solution temperature (LCST ∼ 32 °C) in water is one of the mostly studied one.[26,27] It is hydrophilic and soluble in water as individual chains when the solution temperature is lower than its LCST but becomes hydrophobic and insoluble in water at higher temperatures higher than its LCST, resulting in single-chain globules or large multichain aggregates (mesoglobules).[28,29]

Therefore, a combination of PAA and PNIPAM leads to double sensitive copolymers, such as PAA-*b*-PNIPAM block copolymers, that can self-assemble into polymeric micelles or other types of aggregates, depending on temperature, pH, and block length. Both RAFT and ATRP have been used to synthesize this kind of diblock copolymer.[30,31] PAA-*b*-PNIPAM was also investigated as a potential drug carrier.[32] In the current study, we used it as a modal system to investigate the effect of metal ion-adding temperature on the chain association in aqueous solutions by a combination of static and dynamic laser light scattering (LLS); specifically, by adding metal ions before or after the temperature-induced association of PAA-*b*-PNIPAM chains, we like to see differences, if any, in the association kinetics and the resultant aggregates. The choice of Ca^{2+} instead of other divalent cationic metal ions is due to its proper complexation strength so that the chain association is reversible, which makes our experimental study much easier; i.e., we can use one solution to study the heating-induced association and the cooling-induced dissociation in many cycles.

EXPERIMENTAL SECTION

Materials. The inhibitor in monomer *tert*-butyl acrylate (tBA, Sinopharm, 97%) was removed by passing through a basic alumina column, and tBA is then distilled under a reduced pressure (60 °C and 60 mmHg). The initiator azobis(isobutyronitrile) (AIBN, Aldrich, 99%) was recrystallized from ethanol and dried. 1,4-Dioxane (99%) was refluxed several hours and freshly distilled from sodium benzophenone ketyl immediately prior to each use. *N*-Isopropylacrylamide (NIPAM, Eastman Kodak, 97%) was recrystallized three times from a solution of hexane/toluene (1:1). Dichloromethane (DCM) was distilled over CaH_2 just prior to use. 2-Dodecylsulfanylthiocarbonylsulfanyl-2-methylpropionic acid (DMP) was prepared according as described before.[33] Other reagents were also purchased from Sinopharm and used without further purification unless noted otherwise.

$C_{12}H_{25}SC(=S)S-PtBA-C(Me_2)COOH$ (1). A 100 mL Schlenk flask was charged with DMP (0.87 g, 2.3 mmol), AIBN (37 mg, 0.23 mmol), tBA (26.49 g, 0.21 mol), and 1,4-dioxane (30 mL). The flask was degassed by four freeze−pump−thaw cycles, and the polymerization was carried out at 60 °C for 6 h. The flask was immediately immersed into liquid nitrogen to stop the polymerization. The polymer was dissolved in dioxane, and then the polymer was precipitated into a 10-fold excess of a mixture of water and MeOH (50:50, v:v). After drying in a vacuum oven overnight at 40 °C, $C_{12}H_{25}SC(=S)S-PtBA-C(Me_2)COOH$ was obtained.

dx.doi.org/10.1021/ma300629d | *Macromolecules* 2012, 45, 4830−4838

$C_{12}H_{25}SC(=S)S-PNIPAM-b-PtBA-C(Me_2)COOH$ (2). A 100 mL Schlenk flask was charged with macro-RAFT agent **1** (3.50 g, 0.25 mmol), AIBN (3.5 mg, 0.02 mmol), NIPAM (7.01 g, 61.9 mmol), and 1,4-dioxane (21 mL). The flask was degassed by four freeze–pump–thaw cycles, and the polymerization was carried out at 60 °C for 6 h. The flask was immediately immersed into liquid nitrogen to stop the polymerization. The polymer was dissolved in dioxane, and then the polymer was precipitated into 50:50 v:v water:MeOH solution. After drying in a vacuum oven overnight at 40 °C, the diblock copolymers **2** was obtained. Scheme 1 shows the synthesis steps.

$NC(Me_2)C-PNIPAM-b-PtBA-C(Me_2)COOH$ (3). A 500 mL Schlenk flask was charged with polymer **2** (0.40 g, 0.01 mmol), AIBN (164.3 mg, 1.00 mmol), and 1,4-dioxane (5 mL). The flask was degassed by three freeze–pump–thaw cycles, and the reaction was carried out at 80 °C for 15.5 h. The solution was concentrated by evaporation, and then the polymer was precipitated into a 10-fold excess of *n*-hexane. After dried in a vacuum oven overnight at room temperature, a white powder was collected.

$NC(Me_2)C-PNIPAM-b-PAA-C(Me_2)COOH$ (4). The diblock copolymer **3** were dissolved in dichloromethane ($C \sim 100$ g/L) and stirred at room temperature with 5 equiv of trifluoroacetic acid. After 24 h, dichloromethane and trifluoroacetic acid were removed by rotating evaporation. The collected polymer dissolved in 0.5 M Na_2CO_3 solution, and then the solution was transferred into presoaked dialysis tubing (MWCO = 3000), dialyzed against deionized water for 3 days. A white solid was collected after freeze-drying. Polymer **5** was synthesized by the same method. The pH values of all the solution used were adjusted to 8.3 by 0.1 M HCl and 0.1 M NaOH, where the amount of NaCl introduced can be neglected. The copolymer concentration was kept at 0.2 mg/mL for all the studied. For the LLS experiments, each solution was clarified with a 0.45 μm Millipore Millex-LCR filter to remove dust. Ca^{2+} was added by dropping in a demanded amount of clarified $CaCl_2$ solution (4.00 mg/mL).

The relative molar mass distributions of resultant polymers were characterized using size exclusion chromatography (SEC, Waters 1515) equipped with three Waters Styragel columns (HR2, HR4, HR6) and a refractive index (RI, Wyatt WREX-02) detector. The linear PS was used as a standard. The elution agent used was THF, and the flow rate was kept at 1.0 mL/min. Figure 1 shows the GPC traces of macromolecular RAFT agent **1** and diblock copolymer before and after the alternation of the chain end, where $M_n = 1.40 \times 10^4$ and 3.57×10^4 g/mol, respectively, and their polydispersity index (M_w/M_n) is 1.08 and 1.12, respectively. The alternation of the end group has nearly no effect on the relative molar mass distribution; i.e., no bimolecular termination occurred during the AIBN treatment.

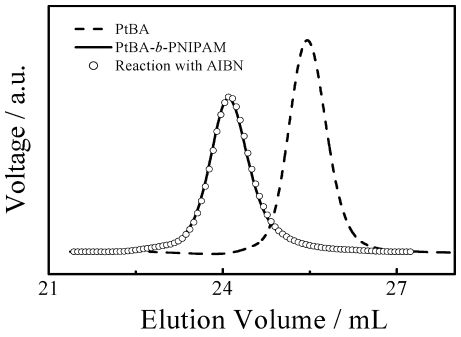

Figure 1. GPC traces of macro-RAFT agent **1** (dashed line), block copolymer **2** (solid line), and $NC(Me_2)C-$ PNIPAM-*b*-PtBA–$C(Me_2)COOH$ (○).

In addition, their compositions were determined from ^{1}H NMR (Figure 2) according to the literature,[30] as shown in Figure 2, where the calculated degree of polymerization is 85 and 181, respectively, for macro-RAFT agent **1** and PNIPAM block of copolymer **2**. By using TFA in dichloromethane, we hydrolyzed the ester group of PtBA-*b*-PNIPAM (polymer **3**). Figure 2 shows that the peak of the methyl ester protons (1.45 ppm) disappears, indicating that all the ester groups of polymer **4** were converted to acrylic acid.[34]

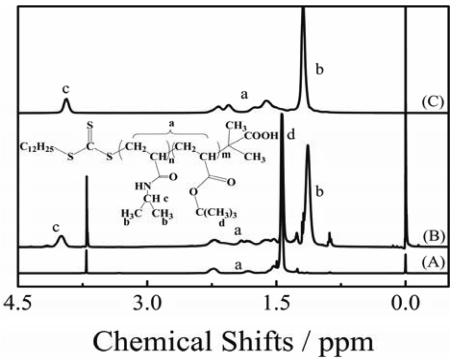

Figure 2. ^{1}H NMR spectra of (A) macro-RAFT agent, PtBA in $CDCl_3$; (B) PtBA-*b*-PNIPAM in $CDCl_3$; and (C) PAA-*b*-PNIPAM in D_2O.

Laser Light Scattering. A commercial LLS spectrometer (ALV/DLS/SLS-5022F) equipped with a multi-τ digital time correlator (ALV5000) and a cylindrical 22 mW UNIPHASE He–Ne laser (λ_0 = 632.8 nm) as the light source was used. In static LLS,[35,36] the angular dependence of the absolute excess time-average scattering intensity, known as the Rayleigh ratio $R_{VV}(q)$, can lead to the weight-average molar mass (M_w), the root-mean-square gyration radius $\langle R_g^2\rangle_z^{1/2}$ (or simply written as $\langle R_g\rangle$), and the second virial coefficient A_2 by using

$$\frac{KC}{R_{VV}(q)} \cong \frac{1}{M_w}\left(1 + \frac{1}{3}\langle R_g^2\rangle_Z q^2\right) + 2A_2C \quad (1)$$

where $K = 4\pi^2(dn/dC)^2/(N_A\lambda_0^4)$ and $q = (4\pi/\lambda_0)\sin(\theta/2)$ with C, dn/dC, N_A, and λ_0 being concentration of the polymer solution, the specific refractive index increment, Avogadro's number, and the wavelength of light in a vacuum, respectively. In our study, the solution was dilute and the extrapolation of $C \to 0$ cannot be done; the term of $2A_2C$ can be ignored. It is worth noting that the calculations of $\langle R_g^2\rangle$ of diblock copolymers and homopolymers are different. In the current study, we have ignored such a difference because the effect is small.

In dynamic LLS,[37] the Laplace inversion of each measured intensity–intensity time correlation function $G^{(2)}(q,t)$ in the self-beating mode can lead to a line-width distribution $G(\Gamma)$, where q is the scattering vector. For dilute solutions, Γ is related to the translational diffusion coefficient D by $(\Gamma/q^2)_{q\to0,C\to0} \to D$. Therefore, $G(\Gamma)$ can be converted into a translational diffusion coefficient distribution $G(D)$ or further a hydrodynamic radius distribution $f(R_h)$ via the Stokes–Einstein equation, $R_h = (k_BT/6\pi\eta_0)/D$, where k_B, T, and η_0 are the Boltzmann constant, the absolute temperature, and the solvent viscosity, respectively. For linear polymer chains with a polydispersity index of $M_w/M_n < 2$, we are able to estimate the polydispersity index by using $M_w/M_n \approx (1 + 4\mu_2/\langle\Gamma\rangle^2)$, where $\mu_2 = \int_0^\infty G(\Gamma)(\Gamma - \langle\Gamma\rangle)^2 d\Gamma$.[38] The dn/dC value of 0.17 mL/g was used to estimate the weight-average molar mass (M_w), which was calculated from the values of PNIPAM and PAA by using the additive weighting rule. All the data listed hereafter were obtained from the extrapolation of $q \to 0$.

RESULTS AND DISCUSSION

First, we studied the micelle formation of $C_{12}H_{25}SC(=S)S-$PNIPAM-*b*-PAA (copolymer **5**) in aqueous solutions by dynamic LLS. Figure 3 shows that its average hydrodynamic radius is ~90 nm, much larger than the size expected for polymeric micelles made of diblock copolymer chains with a relative number-average molar mass of 3.57×10^4 g/mol.[31] In addition, such formed polymeric micelles are also unexpectedly broadly distributed with $\mu_2/\langle\Gamma\rangle^2 = 0.13$ at $\theta = 15°$. We attributed such an abnormal association behavior to their large

dx.doi.org/10.1021/ma300629d | Macromolecules 2012, 45, 4830–4838

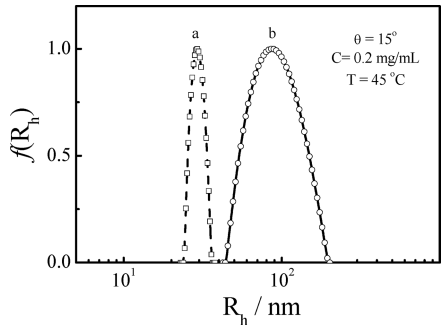

Figure 3. Hydrodynamic radius distributions of (a) $NC(Me_2)C-PNIPAM-b-PAA-C(Me_2)COOH$ and (b) $C_{12}H_{25}SC(=S)S-PNIPAM-b-PAA-C(Me_2)COOH$.

hydrophobic end group introduced by the RAFT agent because it could lead to possible irregular chain association instead of the formation of spherical core−shell micelles.[39]

Therefore, we decided to remove the large RAFT end group and replace it with a small one; namely, $NC(Me_2)C-PNIPAM-b-PtBA-C(Me_2)COOH$, by treating polymer **2** with an excess amount of AIBN according to a method described before.[40] The UV spectrum in Figure 4 shows that the trithiocarbonate

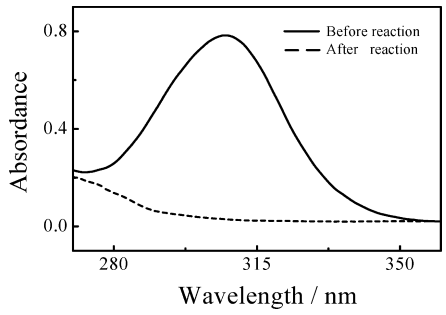

Figure 4. UV spectra of $C_{12}H_{25}SC(=S)S-PNIPAM-b-PtBA-C(Me_2)COOH$ (solid line) and $NC(Me_2)C-PNIPAM-b-PtBA-C(Me_2)COOH$ (dashed line) in THF at the concentration of 2 mg/mL.

peak (~310 nm) disappears after the AIBN treatment.[41] As shown in Figure 3, after the removal of the large hydrophobic end group, the copolymer chains (polymer **4**) self-assemble into smaller and narrowly distributed aggregates with an average hydrodynamic radius of ~31 nm, a clear signature of block copolymer micelles.

Figure 5 summarizes the temperature dependence of the average hydrodynamic radius $\langle R_h \rangle$ and the average aggregation number N_{agg} of PAA-*b*-PNIPAM in an aqueous solution. Our dynamic LLS results reveal a slow relaxation mode even at temperatures lower than the LCST. Presumably, it might be attributed to interchain hydrogen bonding or the long-range interaction of charged chains in salt-free solutions.[31] It has not been completely resolved about the nature of such a slow mode. We will not discuss it further in the current study. At temperatures higher than ~37 °C, polymeric micelles are formed, presumably with a core made of collapsed PNIPAM blocks and a shell made of swollen PAA blocks on its periphery.

Figure 5 shows that further increase of the solution temperature leads to smaller polymeric micelles but the average number of aggregation N_{agg} still increases over the same temperature range, where N_{agg} is defined as $M_{w,agg}/M_{w,chain}$, $M_{w,agg}$, and $M_{w,chain}$ are the weight-average molar masses of

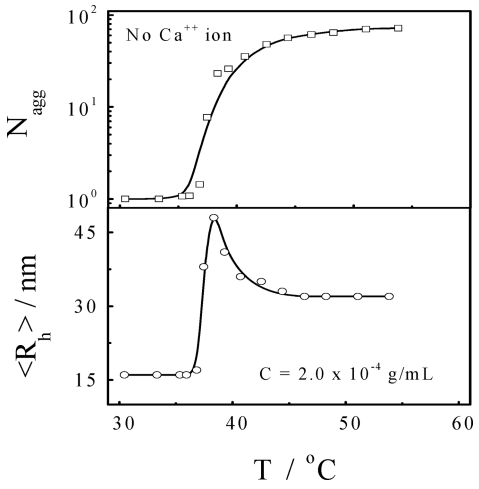

Figure 5. Temperature dependence of average hydrodynamic radius ($\langle R_h \rangle$) and average number of aggregation (N_{agg}) of PAA-*b*-PNIPAM in aqueous solution.

polymeric micelles and individual block copolymer chains, respectively. Presumably, further increase of the solution temperature over ~37 °C has two opposite effects on the measured size of polymeric micelles as follows.

Namely, further increase of the temperature, on the one hand, drives more copolymer chains into each polymeric micelle, increasing its size, but, on the other hand, leads to further shrinking of the PNIPAM core, as schematically shown in Figure 6. This is exactly why $\langle R_h \rangle$ decreases but N_{agg} increases when T is higher than ~39 °C. After knowing the behaviors of PAA-*b*-PNIPAM chains in aqueous solutions, we moved to investigate how the addition of Ca^{2+} at different temperatures affects the chain association. First, different amounts of Ca^{2+} ions were added at 25 °C, and then the solution temperature was jumped to 45 °C.

Figure 7 shows that when $[Ca^{2+}]/[COO^-] < 2$, the average number of aggregation only slightly increases but the average hydrodynamic radius nearly remains a constant as more Ca^{2+} ions are added. As expected, each Ca^{2+} ion can complex with two COO^- groups. At lower ratios of $[Ca^{2+}]/[COO^-]$, the complexation mostly occurs inside each polymeric micelle and makes each hydrophilic PAA block less soluble so that the PAA shell shrinks. On the other hand, each less soluble PAA chain in the shell stabilizes a smaller surface area so that more PNIPAM blocks are inserted into the core, which explains why the average chain density ($\langle \rho \rangle$), defined as $M_{w,agg}/(N_A 4\pi \langle R_h \rangle^3/3)$, increases. The shrinking of the PAA shell and the insertion of more PNIPAM blocks into the core have opposite effects on the size of each polymeric micelle so that $\langle R_h \rangle$ nearly remains a constant but N_{agg} gradually increases with $[Ca^{2+}]/[COO^-]$. At higher $[Ca^{2+}]/[COO^-]$ ratios, the intermicelle complexation starts to occur so that both N_{agg} and $\langle R_h \rangle$ quickly increase but $\langle \rho \rangle$ decreases, indicating that polymeric micelles are connected by the intermicelle complexation between one Ca^{2+} and two COO^- groups on two different micelles. A comparison of Figures 5 and 7 shows that both N_{agg} and $\langle R_h \rangle$ become significantly larger when a large amount of Ca^{2+} ions are added because the intermicelle complex leads to the formation of a loosely connected micelle clusters.

Figure 8 shows kinetics of thermally induced aggregation of PAA-*b*-PNIPAM copolymer chains in the presence of the Ca^{2+}/COO^- complexation in terms of the time dependence of both

dx.doi.org/10.1021/ma300629d | Macromolecules 2012, 45, 4830−4838

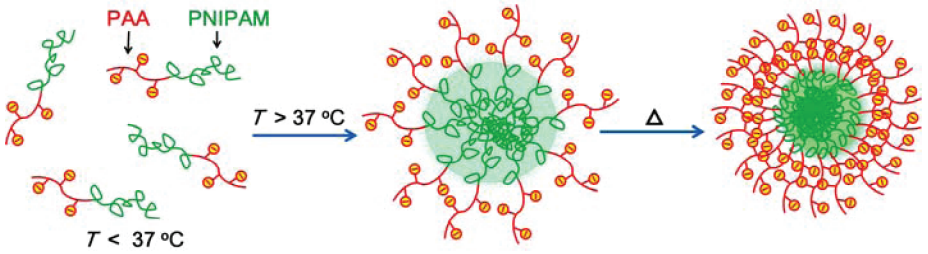

Figure 6. Schematic of temperature-induced formation of a polymeric micelle made of thermally sensitive linear PAA-*b*-PNIPAM diblock copolymer chains.

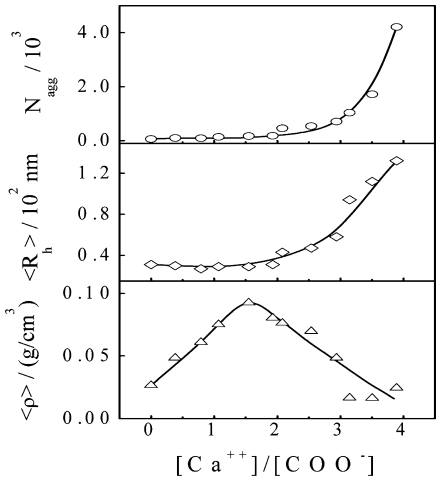

Figure 7. Ca^{2+} concentration dependence of average number of aggregation (N_{agg}), average hydrodynamic radius ($\langle R_h \rangle$), and chain density ($\langle \rho \rangle$) of aggregates made of PAA-*b*-PNIPAM chains in an aqueous solution at 45 °C, where Ca^{2+} ions were added at 25 °C before temperature was jumped to 45 °C and data were collected 5 h after temperature jump.

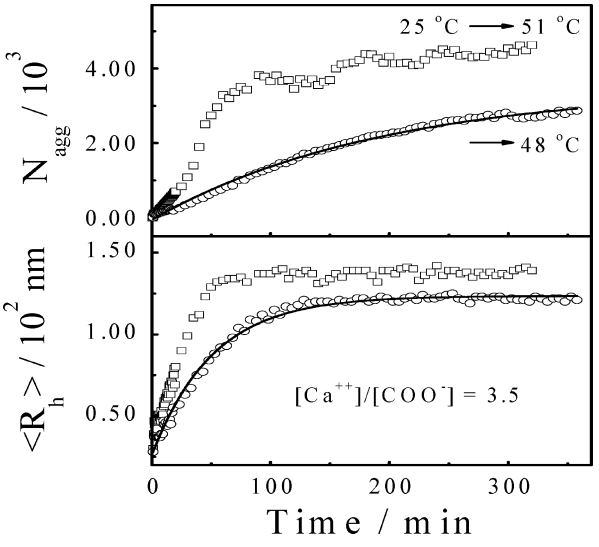

Figure 8. Time dependence of average aggregation number (N_{agg}) and average hydrodynamic radius ($\langle R_h \rangle$) of aggregates made of PAA-*b*-PNIPAM copolymer chains, where Ca^{2+} ions were added at 25 °C before solution temperature was jumped to desired aggregation temperatures and lines represent the single-exponential fitting, where θ = 15°.

N_{agg} and $\langle R_h \rangle$ of the resultant aggregates. The aggregation slows down after a few hours and gradually approaches a plateau. It is worth noting that these resultant aggregates were stable, and no precipitation was observed over a long time period. It is clear that a higher temperature leads to a fast aggregation process and results in larger aggregates. It is known that PNIPAM becomes more hydrophobic, and more copolymer chains are packed inside each aggregate as the aggregation temperatures increases, as shown in Figure 5. Therefore, more COO^- groups are on its periphery, increasing the sticking probability, which explains the results in Figure 8. On the other hand, one should also note that the complexation between two COO^- and one Ca^{2+} ions is mainly an entropy-driven process.[42] Therefore, the increase of temperature decreases the free energy and favors the complexation. The aggregation kinetics can be described by a single-exponential function, except the very initial stage (shown by the lines). The initial fast process is related to the association of individual chains and the formation of micelles or micelle-like clusters, while the data in Figure 8 mainly reflect the micelle−micelle (cluster−cluster) aggregation.

Figure 9 shows that in the heating process both $\langle R_h \rangle$ and N_{agg} sharply increase when the temperatures higher than the

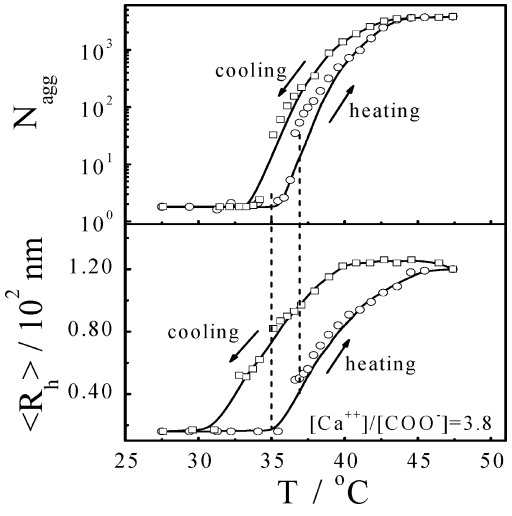

Figure 9. Temperature dependence of average number of aggregation (N_{agg}) and average hydrodynamic radius ($\langle R_h \rangle$) of aggregates made of PAA-*b*-PNIPAM chains in an aqueous solution, where Ca^{2+} ions were added at 25 °C before solution was slowly heated to higher temperatures.

assembly temperature (35−36 °C), revealing the intermicelle association. A comparison of Figures 5 and 9 shows that without Ca^{2+}, the interchain association starts at ~37 °C, but in the presence of Ca^{2+}, both $\langle R_h \rangle$ and N_{agg} start to increase at ~35 °C, indicating that Ca^{2+} induces the association of a limited number of copolymer chains to form the premicelle

dx.doi.org/10.1021/ma300629d | *Macromolecules* 2012, 45, 4830−4838

association or micelles between ~35 and ~37 °C (marked by two dashed lines in Figure 9). Further increase of the solution temperature leads to the formation of more polymeric micelles and the intermicelle association so that both $\langle R_h \rangle$ and N_{agg} increase. The aggregation stops at temperatures higher than ~45 °C, and $\langle R_h \rangle$ and N_{agg} approach ~120 nm and ~3800, respectively, indicating the formation of stable micelle aggregates.

There is a clear hysteresis between the cooling and heating processes, especially for $\langle R_h \rangle$. It is interesting to see that in the cooling process $\langle R_h \rangle$ remains a constant, but N_{agg} decreases in the temperature range 45−40 °C. Note that as the solution temperature decreases, individual polymeric micelles (the PNIPAM core) swell; i.e., their size increases (as shown in Figure 5), and at the same time, the aggregates made of polymer micelles start to dissociate into smaller ones. Two processes have opposite effects on the measured $\langle R_h \rangle$, which explains why there is nearly no change in $\langle R_h \rangle$ but N_{agg} decreases. A similar hysteresis was also observed in the coil-to-globule-to-coil transition of individual PNIPAM chains during the heating-and-cooling cycle, which was attributed to the later confirmed formation of some additional intrachain hydrogen bonds when PNIPAM are in its collapsed state.[29,43−46] When the solution is cooled to ~33 °C, N_{agg} returns to its initial value but $\langle R_h \rangle$ only decreases to ~50 nm, which further supports our previous discussion; namely, the Ca^{2+}/COO^- complexation mainly leads to the interchain association but not the formation of polymeric micelles in the temperature range 35−37 °C. Finally, $\langle R_h \rangle$ returns to its original value at ~31 °C, indicating the disintegration of those associated copolymer chains. The Ca^{2+}-induced aggregation of PAA-*b*-PNIPAM chains and polymeric micelles is controllable and reversible.

In order to avoid the interference of Ca^{2+}-induced chain association before the formation of polymeric micelles and concentrate on the intermicelle aggregation, we heated the copolymer solution to a temperature much higher than the micelle temperature (~37 °C) before adding Ca^{2+} ions and characterized the resultant intermicelle aggregates. Figure 10

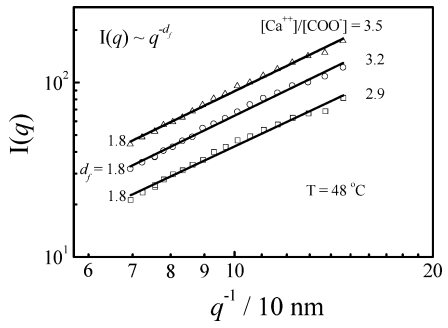

Figure 10. Scattering vector (q) dependence of scattering intensity ($I(q)$) of micelle aggregates formed at different Ca^{2+} concentrations, where Ca^{2+} ions were added after copolymer solution was heated to 48 °C.

shows that the time-average scattering intensity $I(q)$ is scaled to the scattering vector q as $I(q) \propto q^{-d_f}$ with $d_f = 1.8 \pm 0.1$, independent of the Ca^{2+} concentration, revealing that the Ca^{2+}-induced intermicelle aggregation follows the DLCA process. We should note that the straight line within one order of q is only a necessary condition not a sufficient one. To really establish a object with a fractal structure, one should use at least three orders of q. Readers should be aware of this important fact. As expected, $I(q)$ increases with the Ca^{2+} concentration because more polymeric micelles are "connected" by more Ca^{2+} ions via the Ca^{2+}/COO^- complexation. Note that the aggregation was too fast to be followed by our current LLS instrument so that we were not able to study the kinetics of such a process.

Further, Figure 11 shows that d_f slightly increases from 1.7 to 1.9 when the aggregation temperature decreases from 51 to 45

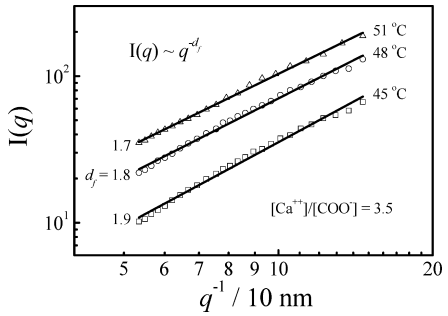

Figure 11. Scattering vector (q) dependence of scattering intensity ($I(q)$) of micelle aggregates formed at different temperatures, where Ca^{2+} ions were added after solution was jumped to each desired temperature.

°C. In general, d_f decreases as the sticking probability increases. At a higher temperature, PNIPAM becomes more hydrophobic and more copolymer chains are inserted in each micelle, as shown in Figure 5. In this way, more COO^- groups are expected to be on the periphery of each micelle and the PAA chains on the shell are more extended so that the Ca^{2+}-induced sticking probability should increase with the aggregation temperature, which explains the decrease of d_f as the temperature increases in Figure 11.

We also added Ca^{2+} ions before the solution was jumped to each desired temperature. A comparison of Figures 11 and 12

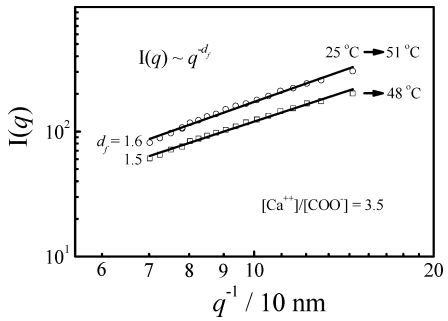

Figure 12. Scattering vector (q) dependence of scattering intensity ($I(q)$) of micelle aggregates formed at different temperatures, where Ca^{2+} ions were added before solution was jumped to each desired temperature.

shows that adding Ca^{2+} ions before the temperature jump leads to a lower fractal dimension, i.e., resulting in slightly looser aggregates with a more open structure, but still follows the DLCA process. Such a difference is due to the formation of interchain Ca^{2+}/COO^- complexes before they are assembled into polymeric micelles during the heating. As expected, two chains interconnected by the Ca^{2+}/COO^- complexation have a

dx.doi.org/10.1021/ma300629d | Macromolecules 2012, 45, 4830−4838

higher chance to be assembled into two different resultant micelles to bring them together.

In other words, the interchain Ca^{2+}/COO^- complexation before the micelles formation increases the sticking probability among different micelles and slightly reduces d_f. Figure 13

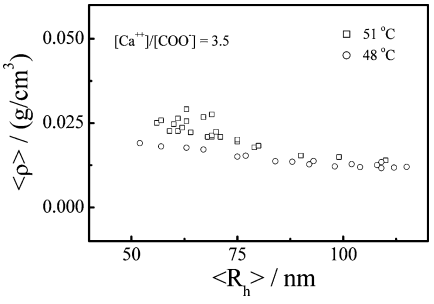

Figure 13. Average hydrodynamic radius ($\langle R_h \rangle$) dependence of average chain density ($\langle \rho \rangle$) of micelle aggregates formed at two temperatures.

shows that the average chain density ($\langle \rho \rangle$) decreases as the aggregation proceeds, revealing that larger aggregates become looser and less uniform and further reflecting the DLCA nature. It also shows that a higher aggregation temperature leads to a high chain density. As shown in Figure 5, a high aggregation temperature leads to a higher aggregation number but has less effect on the aggregate size. A comparison of Figures 5 and 13 shows that such a difference is mainly due to the chain density difference inside individual micelles formed at different temperatures, not related to the aggregation among different polymeric micelles even though there is a slight increase of d_f from 1.5 to 1.6, as shown in Figure 12.

Figures 11 and 12 reveal the differences when the order of adding Ca^{2+} ions and the temperature jump. We have shown in Figure 11 that the d_f slightly decreases as the temperature increases, when Ca^{2+} was added after the solution was jumped to desired temperature. In contrast to Figure 11, Figure 12 shows that d_f increases with the aggregation temperature when Ca^{2+} ions are added before the temperature jump. Note that two copolymer chains interconnected by the Ca^{2+}/COO^- complexation can end up in one micelle or two different micelles during the temperature jump, i.e., the intramicelle or intermicelle self-assembly. When the solution is jumped to a higher temperature, the micelle-formation kinetics is much fast, as shown in Figure 8, so that two interconnected copolymer chains have a much higher chance to undergo the intramicelle self-assembly to form some PAA "loops" in the shell. The formation of these "loops" on the periphery of each micelle reduces both the Ca^{2+} and COO^- groups for the intermicelle complexation so that the sticking probability decreases, which explains why d_f increases with the aggregation temperature. The slightly difference between adding Ca^{2+} ions before and after the temperature jump is schematically summarized in Figure 14.

In order to further demonstrate that the effect of metal ions on the stability of charged polymer chains in dilute solutions, such as proteins in aqueous solutions, we prepared a thermally sensitive linear copolymer Poly(NIPAM-*co*-AA) and studied its association in water without and with an equal molar amount of Cu^{2+}. Intuitively, one Cu^{2+} cation can bind to two $-COO^-$ anions on one copolymer chain or on two copolymer chains. The interchain complexation should lead to more aggregation, resulting in larger particles, at higher temperatures. However, Figures 15 and 16 reveal that in the presence of Cu^{2+} ions the

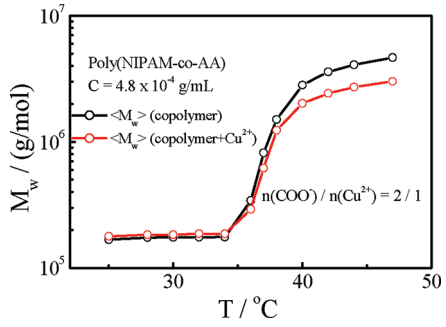

Figure 15. Temperature dependence of weight-average molar mass (M_w) of P(NIPAM-*co*-AA) copolymer in aqueous solutions.

copolymer chains tend to aggregate less and form smaller particles in terms of either $\langle R_g \rangle$ or $\langle R_h \rangle$. Note that the *Y*-axis in Figure 15 is logarithmically scaled. Therefore, the difference in M_w at higher temperatures is much more profound; specifically

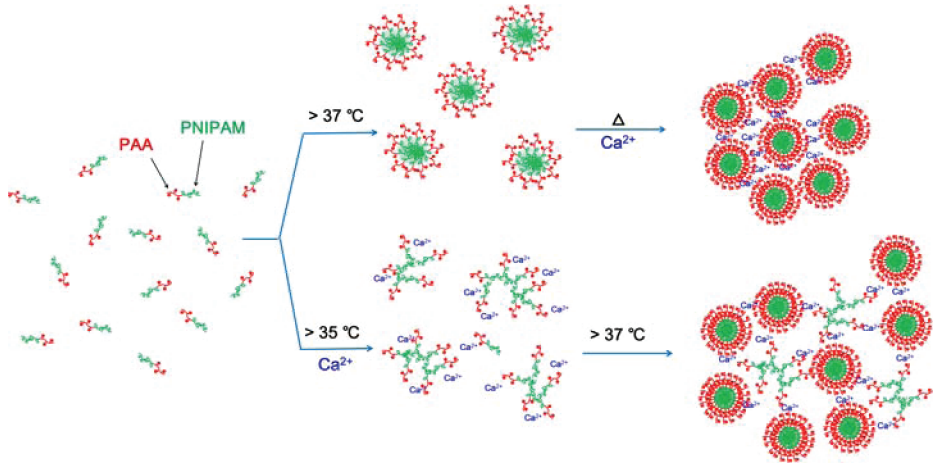

Figure 14. Schematic of effect of adding Ca^{2+} ions before and after temperature jump on Ca^{2+}/COO^- complexation-induced micelle aggregation of thermally sensitive PAA-*b*-PNIPAM copolymer chains, where micelle temperature is ~37 °C.

dx.doi.org/10.1021/ma300629d | *Macromolecules* 2012, 45, 4830−4838

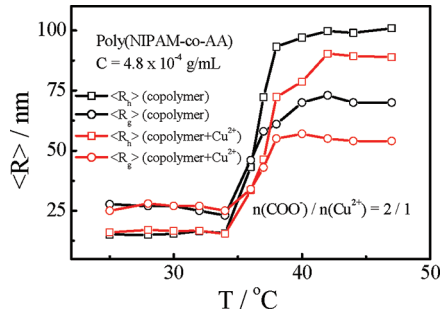

Figure 16. Temperature dependence of average hydrodynamic radius ($\langle R_h \rangle$) and average radius of gyration ($\langle R_g \rangle$) of P(NIPAM-*co*-AA) copolymer.

at 47 °C, the aggregation numbers are ~27 and ~16, respectively, without and with adding Cu^{2+} ions.

On the other hand, Figure 17 shows that Cu^{2+} has less an effect on the ratio of $\langle R_g \rangle / \langle R_h \rangle$, indicating that the structure

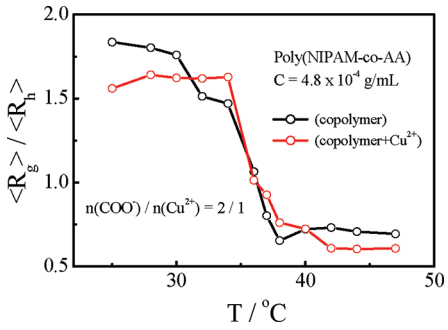

Figure 17. Temperature dependence of ratio of average radius of gyration to average hydrodynamic radius $\langle R_g \rangle / \langle R_h \rangle$ of P(NIPAM-*co*-AA) copolymer.

and conformation of the aggregated chains are similar. A combination of Figures 15–17 reveals that Cu^{2+} mainly induces the intrachain complexation that actually "freezes" and stabilizes the chain conformation so that the copolymer chains have less chance to undergo the interchain aggregation/association. Such an unexpected stabilization mechanism can be qualitatively argued in terms of the viscoelastic effect described before,[47] which might indirectly explain why some prion diseases occur in the place where its soil contains less Cu^{2+} ions.

CONCLUSION

The large end group introduced into each poly(*tert*-butyl acrylate)-*b*-poly(*N*-isopropylacrylamide) (PtBA-*b*-PNIPAM) chain in sequential RAFT polymerization can affect the micelle formation of such block copolymer chain in a selective solvent. The hydrolysis of PtBA-*b*-PNIPAM into PAA-*b*-PNIPAM can lead to narrowly distributed diblock copolymer chains with one charged block and one thermally sensitive block so that they can self-assemble into well-defined spherical polymeric micelles with a core and a shell respectively made of collapsed PNIPAM chains and swollen PAA chains at temperatures higher than 37 °C. Our results demonstrate that the presence of Ca^{2+} ions and the Ca^{2+}/COO^- complexation can flocculate individual polymeric micelles together to form large and loosely connected micelle clusters. The addition of Ca^{2+} ions before or after the temperature jump from room temperature to temperatures much higher than the micelle formation temperature affects the interchain and intermicelle association. Namely, when Ca^{2+} ions were added after solution was jumped to each desired temperature, the Ca^{2+}/COO^- complexation mainly induces the aggregation of resultant polymeric micelles; while when Ca^{2+} ions were added before the temperature jump, the copolymer chains first associate together to form small loose interchain aggregates before they are incorporated into the micelles (intramicelle or intermicelle) at higher temperatures, resulting in a lower fractal dimension and a lower average chain density per micelle aggregate. The Ca^{2+}/COO^- complexation induced intermicelle association essentially follows the DLCA process even thought the temperature, the Ca^{2+} concentration and the sequence of adding Ca^{2+} ions and heating the copolymer solution lead to different aggregation rates, cluster sizes, and structures. The current study provides a model system to further investigate a more complicate problem—the effect of metal ions on the stability of protein chains.

ASSOCIATED CONTENT

Supporting Information

Figures S1 and S2. This material is available free of charge via the Internet at http://pubs.acs.org.

AUTHOR INFORMATION

Corresponding Author

*The Hong Kong address should be used for correspondence. E-mail: chiwu@cuhk.edu.hk.

Notes

The authors declare no competing financial interest.

ACKNOWLEDGMENTS

The financial support of the National Natural Scientific Foundation of China Projects (20934005 and 51173177), the Ministry of Science and Technology of China (Key Project, 2012CB933802), and the Hong Kong Special Administration Region Earmarked Projects (CUHK4042/10P, 2130241, 2060405; and CUHK4036/11P, 2130281, 2060431) is gratefully acknowledged.

REFERENCES

(1) Watson, L. In *Encyclopedia of Surface and Colloid Science*, 2nd ed.; Somasundaran, P., Ed.; Taylor & Francis: New York, 2006; Vol. *2*, pp 1014–1025.
(2) Huber, K. *J. Phys. Chem.* **1993**, *97*, 9825–9830.
(3) Schweins, R.; Huber, K. *Eur. Phys. J. E* **2001**, *5*, 117–126.
(4) Lages, S.; Schweins, R.; Huber, K. *J. Phys. Chem. B* **2007**, *111*, 10431–10437.
(5) Lages, S.; Michels, R.; Huber, K. *Macromolecules* **2010**, *43*, 3027–3035.
(6) Förster, S.; Abetz, V.; Müller, A. H. E. In *Polyelectrolytes with Defined Molecular Architecture II*; Schmidt, M., Ed.; Springer: Berlin, 2004; Vol. *166*, pp 267–277.
(7) Brown, D. R.; Qin, K.; Herms, J. W.; Madlung, A.; Manson, J.; Strome, R.; Fraser, P. E.; Kruck, T.; von Bohlen, A.; Schulz-Schaeffer, W.; Giese, A.; Westaway, D.; Kretzschmar, H. *Nature* **1997**, *390*, 684–687.
(8) Hussein, M. F.; Al-Mufarrej, S. I. *Sci. J. King Faisal Univ. (Basic Appl. Sci.)* **2004**, *5*, 139–166.
(9) BSE proteins may cause fatal insomnia: http://news.bbc.co.uk/2/hi/health/355297.stm (May 28, 1999).
(10) Meakin, P. *Phys. Rev. Lett.* **1983**, *51*, 1119–1122.
(11) Martin, J. E.; Ackerson, B. J. *Phy. Rev. A* **1985**, *31*, 1180–1182.

(12) Jullien, R.; Botet, R.; Mors, P. M. *Faraday Discuss. Chem. Soc.* **1987**, *83*, 125−137.
(13) Reinecke, H.; Fazel, N.; Dosiere, M.; Guenet, J.-M. *Macromolecules* **1997**, *30*, 8360−8364.
(14) Aubert, C.; Cannell, D. S. *Phys. Rev. Lett.* **1986**, *56*, 738−741.
(15) Tang, P.; Colflesh, D. E.; Chu, B. *J. Colloid Interface Sci.* **1988**, *126*, 304−313.
(16) Lin, M. Y.; Lindsay, H. M.; Weitz, D. A.; Ball, R. C.; Klein, R.; Meakin, P. *Nature* **1989**, *339*, 360−362.
(17) Micali, N.; Mallamace, F.; Romeo, A.; Purrello, R.; Monsù Scolaro, L. *J. Phys. Chem. B* **2000**, *104*, 5897−5904.
(18) Zhou, Z.; Chu, B. *J. Colloid Interface Sci.* **1991**, *143*, 356−365.
(19) Weitz, D. A.; Huang, J. S.; Lin, M. Y.; Sung, J. *Phys. Rev. Lett.* **1985**, *54*, 1416−1419.
(20) Aymard, P.; Nicolai, T.; Durand, D.; Clark, A. *Macromolecules* **1999**, *32*, 2542−2552.
(21) Kim, A. Y.; Berg, J. C. *Langmuir* **1999**, *16*, 2101−2104.
(22) Takata, S.-i.; Norisuye, T.; Tanaka, N.; Shibayama, M. *Macromolecules* **2000**, *33*, 5470−5475.
(23) Pelletier, O.; Davidson, P.; Bourgaux, C.; Coulon, C.; Regnault, S.; Livage, J. *Langmuir* **2000**, *16*, 5295−5303.
(24) Nakata, M.; Nakagawa, T.; Nakamura, Y.; Wakatsuki, S. *J. Chem. Phys.* **1999**, *110*, 2711−2716.
(25) Dai, S.; Ravi, P.; Tam, K. C. *Soft Matter* **2008**, *4*, 435−449.
(26) Otake, K.; Inomata, H.; Konno, M.; Saito, S. *Macromolecules* **1990**, *23*, 283−289.
(27) Kubota, K.; Fujishige, S.; Ando, I. *J. Phys. Chem.* **1990**, *94*, 5154−5158.
(28) Wu, C.; Zhou, S. *Phys. Rev. Lett.* **1996**, *77*, 3053−3055.
(29) Wu, C.; Wang, X. *Phys. Rev. Lett.* **1998**, *80*, 4092−4094.
(30) Li, G.; Song, S.; Guo, L.; Ma, S. *J. Polym. Sci., Part A: Polym. Chem.* **2008**, *46*, 5028−5035.
(31) Schilli, C. M.; Zhang, M.; Rizzardo, E.; Thang, S. H.; Chong, Y. K.; Edwards, K.; Karlsson, G.; Müller, A. H. E. *Macromolecules* **2004**, *37*, 7861−7866.
(32) Li, G.; Guo, L.; Ma, S. *J. Appl. Polym. Sci.* **2009**, *113*, 1364−1368.
(33) Lai, J. T.; Filla, D.; Shea, R. *Macromolecules* **2002**, *35*, 6754−6756.
(34) Ma, Q. G.; Wooley, K. *J. Polym. Sci., Part A: Polym. Chem.* **2000**, *38*, 4805−4820.
(35) Chu, B. *Laser Light Scattering*, 2nd ed.; Academic Press: New York, 1991.
(36) Zimm, B. H. *J. Chem. Phys.* **1948**, *16*, 1099−1116.
(37) Berne, B. J.; Pecroa, R. *Dynamic Light Scattering*; Plenum Press: New York, 1976.
(38) Wu, C. *Macromolecules* **1993**, *26*, 3821−3825.
(39) Loiseau, J.; Doërr, N.; Suau, J. M.; Egraz, J. B.; Llauro, M. F.; Ladavière, C.; Claverie, J. *Macromolecules* **2003**, *36*, 3066−3077.
(40) Perrier, S.; Takolpuckdee, P.; Mars, C. A. *Macromolecules* **2005**, *38*, 2033−2036.
(41) Qiu, X.-P.; Winnik, F. M. *Macromolecules* **2007**, *40*, 872−878.
(42) Sinn, C. G.; Dimova, R.; Antonietti, M. *Macromolecules* **2004**, *37*, 3444−3450.
(43) Maeda, Y.; Higuchi, T.; Ikeda, I. *Langmuir* **2000**, *16*, 7503−7509.
(44) Maeda, Y.; Nakamura, T.; Ikeda, I. *Macromolecules* **2001**, *34*, 1391−1399.
(45) Liu, G. M.; Zhang, G. Z. *J. Phys. Chem. B* **2005**, *109*, 743−747.
(46) Cheng, H.; Shen, L.; Wu, C. *Macromolecules* **2006**, *39*, 2325−2329.
(47) Zhang, G. Z.; Wu, C. *Adv. Polym. Sci.* **2006**, *195*, 101−176.